International Journal of Engineering

Journal Homepage: www.ije.ir

# Physical Modelling of a Strip Footing on a Geosynthetic Reinforced Soil Wall Containing Tire Shred Subjected to Monotonic and Cyclic Loading

M. H. Hoseini, A. Noorzad*, M. Zamanian

*Faculty of Civil, Water and Environmental Engineering, Shahid Beheshti University, Tehran, Iran*

*P A P E R I N F O*

*Paper history:*
Received 5 May 2021
Received in revised form 9 July 2021
Accepted 22 July 2021

*Keywords*:
*Geosynthetic Reinforced Wall*
*Physical Modeling*
*Strip Footing*
*Tire Shred*
*Bearing Capacity*

*A B S T R A C T*

In this study, the mechanical behavior of geosynthetic reinforced soil walls was investigated through physical modeling subjected to strip footing monotonic and cyclic loads at various stress paths. The influence of footing location, stress level, post-cyclic behavior and sand-tire shred admixture on the lateral deformations of the wall facing, bearing capacity and the settlement beneath the footing were assessed. To this aim, 12 physical model tests were conducted on a scale of 1: 4. Results indicated that the bearing capacity has increased with an increase in the offset distance of the strip footing to the wall facing and adding tire shred to the backfill material; but an increase is more prominent by adding tire shred to the backfill material. The location of the footing from the wall facing was a crucial parameter on the deformation of facing and the failure mode of the footing. Failure in the facing was the predominant mode of failure in the near facing footing. However, a rupture in the geosynthetic caused failure in the footing far from facing footing. Also, the results of cyclic loading tests showed both permanent displacement and residual settlement accumulated with load cycles and a majority of them occurred over the first fifteen cycles. Depending on where strip footing was located, it may or may not induce a magnifying effect on subsequent cyclic loading responses.

***doi**: 10.5829/ije.2021.34.10a.08*

## 1. INTRODUCTION

Using geosynthetic materials to increase the tensile load of the soil has been widely reported in recent decades [1-3]. Geosynthetic reinforced soil (GRS) walls are one of the traditional structures that are based on these types of materials. From the environmental point of view, GRS walls have been attracted due to higher flexibility, construction time, cost effectiveness and the possibility of using local materials.

Several experimental and numerical studies sought to investigate the monotonic and cyclic behavior of GRS walls. Among them, the effects of toe resistance [4, 5], backfill relative density [6, 7], facing inclination [8], the facing existence [9], the location and the value of the surcharge load on lateral deformations [10-14], backfill materials [15-17] and wall geometry on failure mode [18] are the most important parameters that have been reported in the literatures. The results of those works showed that by increasing the frictional resistance of the wall toe, the soil density, the surface angle to the vertical axis, and the load distance from the facing, the static bearing capacity of the wall increases, while the lateral deformations decrease. Another major finding is that the properties of the backfill soil and reinforcement layers have little influence on the geometry of the failure surface. However, parameters related to the geometry of the wall, such as the size and location of the bridge seating, and the height of the wall, have significant effects. In contrast to the extensive researches on GRS walls under static loading, very limited studies have been conducted on the behavior under cyclic loading conditions.

One of the most fundamental limitations of GRS walls is their limited bearing capacity, which has been estimated to be 192 kPa [19, 20]. Therefore, using materials like tire shred with high ductility properties

*Corresponding Author Institutional Email: a_noorzad@sbu.ac.ir (A. Noorzad)

Please cite this article as: M. H. Hoseini, A. Noorzad, M. Zamanian, Physical Modelling of a Strip Footing on a Geosynthetic Reinforced Soil Wall Containing Tire Shred Subjected to Monotonic and Cyclic Loading, International Journal of Engineering, Transactions A: Basics, Vol. 34, No. 10, (2021) 2266-2279

could enhance the bearing capacity of GRS walls. The performance of tire shreds when mixed with sand has been reported by many researchers [21, 22]. Despite the well-known performance of sand and tire shred mixtures, only a limited number of studies have employed such mixtures in the body of the reinforced soil walls. For instance, Xiao et al. [23] investigated the seismic behavior of a reinforced soil wall constructed by embedding tire shreds using a shaking table. They observed that under similar conditions, walls constructed with tire shreds, compared to the conventional type of reinforced soil walls, had experienced less lateral displacement, vertical settlement, acceleration, and stress.

Most of previous studies have been focused on the monotonic behavior of GRS walls. However, there are few studies directed to investigate the response of GRS walls subjected to cyclic loading. In this line, several uncertainties are associated with the influencial parameters on the failure mode of GRS walls under cyclic loading of a shallow foundation. In addition, few studies investigated the application of shredded tires for increasing the ductility of the GRS walls. Therefore, series of physical models with a scale of 1: 4 have been carried out. The monotonic behavior of these walls was studied and simulated under similar conditions to cyclic loading.

## 2. MATERIALS AND METHODS

**2. 1. Experimental Setup** The model test setup used in this study consist of a rigid soil chamber and a computer-controlled loading system. The length, width, and height of the cubic box are 1600, 400, and 800 mm, respectively. A polystyrene foam layer and a film of clay were placed in the beneath of the box to isolate it from the surrounding environment. A transparent Plexiglas wall (with a thickness of 10 mm) was placed on one side of the wall for visual observation. Figure 1(a) depicts an image of the setup. The stress and displacement of the wall facing and footing settlement was measured using a S-shaped load cell and three LVDTs. The positions of the reinforcement layers and the LVDTs are illustrated in Figure 1(b). For the tests on reduced-scale models in a 1-g gravitational field, similarity relationships must be considered to produce similar responses between model and prototype structures. The similitude relationships proposed by Iai [24] that have been widely used by other researchers [25, 26] have been used for this study. The length scaling factor was selected of 4 and it was referred to as the ratio of the prototype dimensions to the physical model dimensions. The geometry of the model, footing width, stiffness of geosynthetic, applied pressure, frequency and loading time were scaled. The theoretical scaling factors for the similitude relationships are summarized in Table 1.

**2. 2. Soil** Figure 2(a) presents the particle size distribution of the D11 Firuzkuh sand (according to the ASTM D-422-63 standard [27]) and the microscopic images of the grains are presented in Figure 2(b). Poorly-graded dry sand was used in the model tests. This sand was selected to simulate a reduced size and strength backfill. The mean particle size ($D_{50}$) was 1.45mm, while the uniformity coefficient ($C_u$) and the coefficient of curvature ($C_c$) were 1.6 and 1.2, respectively. As shown in Figure 2(b), the sand grains generally have semi-sharp corners (sub-angular to sub-rounded) with medium to low sphericity, as compared to the diagrams proposed by Maroof et al. [28].

(a)

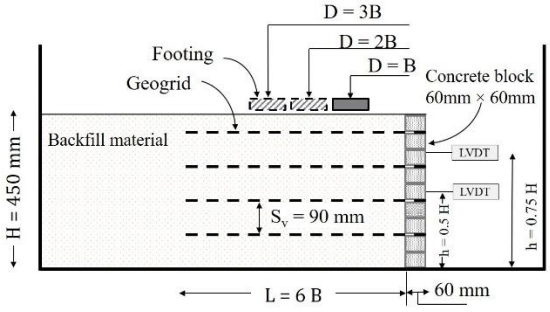


(b)

**Figure 1.** a) Photograph illustrating the Test setup, b) schematic view of apparatus and samples geometry

**TABLE 1.** Similitude relationships for 1-g tests [24]

| Variable | Theoretical scaling factor | Scaling factor for λ=4 |
|---|---|---|
| Length | λ | 4 |
| Material density | 1 | 1 |
| Strain | 1 | 1 |
| Mass | $\lambda^3$ | 64 |
| Stress | λ | 4 |
| stiffness | $\lambda^2$ | 16 |
| Time | $\lambda^{0.5}$ | 2 |
| Frequency | $\lambda^{-0.5}$ | 0.50 |

According to the ASTM D4253 [29] standard, the maximum and minimum unit weights of the sand were 17.8 and 14.3 kN/m$^3$, respectively. In the direct shear test, the friction angle at the target relative density (RD) of 70% was 43 degrees. The obtained specific gravity (Gs) is 2.62. The properties of the soil are summarized in Table 2.

**2. 3. Tire Shred** Based on previous studies, the tire shred can significantly increase the modulus and shear strength of the granular layer [21, 22, 30]. The grain size distribution curve of the tire shred is depicted in Figure 2(a). The tire shred grains have a specific gravity, $G_s$, of 1.16, while the elastic modulus is 3.27 MPa. The tire shred particles were prepared from a truck tire after ensuring that they were free of any steel and cord. In the direct shear test (100 mm ×100 mm box), the friction angle was computed 31 degrees; while the friction angle from the tire shred-geosynthetic interaction became 30 degrees.

**2.4. Reinforcement Layer** According to ASTM [31], the typical tensile strength of the uniaxial geogrid ranges from 58 to 210 kN/m. Based on Table 1, the tensile strength reduces by the square of the scale value. Considering the scale value of 1:4 in this research, the tensile strengths reduced to the ranges of 3.5 to 13 kN/m. A geosynthetic with a 10 mm×10 mm aperture size and a failure tensile strength of 6.1 kN/m in each direction [31] was selected as a reinforcement layer to satisfy the required tensile strength. The aperture size is not highly important, except for the pull-out capacity. However, when the reinforcement length is 0.7 times the wall height, pull-out is often not an issue [19, 20]. In this study, the reinforcement layer length was 510 mm.

**TABLE 2.** Properties of the soil

| Properties | Value |
|---|---|
| Specific gravity, $G_s$ | 2.62 |
| Mean particle size, $D_{50}$ (mm) | 1.45 |
| Effective particle size, $D_{10}$ (mm) | 0.91 |
| Coefficient of uniformity, $C_u$ | 1.6 |
| Coefficient of curvature, $C_c$ | 1.2 |
| Maximum unit weights, $\gamma_{max}$ (kN/m$^3$) | 17.8 |
| Minimum unit weights, $\gamma_{min}$ (kN/m$^3$) | 14.3 |
| Optimum moisture content, (%) | 2.5 |
| Friction angle, $\varphi$(degree) | 43 |
| Friction angle from sand-geosynthetic interaction, (degree) | 36 |
| USCS soil clasification | SP |

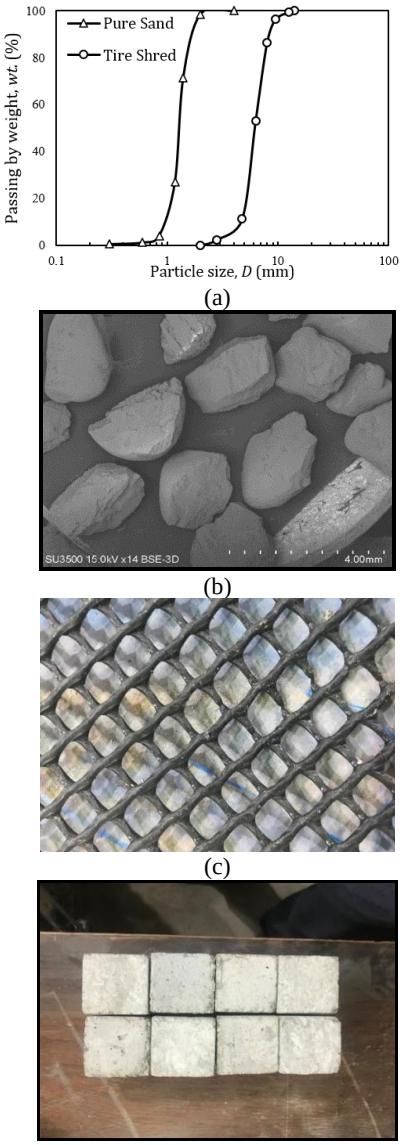


(a) (b) (c) (d)

**Figure 2.** a) Grain size distribution of the sand, b) microscopic view of the grains, c) the geosynthetic, d) the facing block

The physical and mechanical properties of this type of geosynthetic, provided by the factory, are presented in Table 3, further Figure 2(c) shows a photograph of the geosynthetic.

**2. 5. Facing** Concrete blocks with a width of 60 mm, a length of 50 mm, and a height of 45 mm were used to build the facing panels. Figure 2(d) demonstrates the concrete blocks of the facing. According to FHWA [33], the joint between the facing blocks and the reinforcement layers in GRS walls is

**TABLE 3.** Physical and mechanical properties of the geosynthetic

| Physical property | | Mechanical property | |
|---|---|---|---|
| Aperture size (mm) | 10×10 | Ultimate tensile strength (kN/m) | 6.1 |
| Rib thickness (mm) | 3.3 | Maximum strain at maximum strength (%) | 51.7 |
| Weight of unit area ($g/m^2$) | 700 | Tensile strength at 10% strain (kN/m) | 2.9 |
| Polymer material | HDPE | | |

extremely weak. The lateral blocks of the wall facing were greased in order to eliminate the effects of the sidewalls on the sample. There is no connection between the facing and the reinforcement layers, except for the friction between the geosynthetic layers and the facing blocks.

**2. 6. Strip Footing** A metal sheet with a thickness of 25 mm, a width of 75 mm, and a length equal to the width of the box (i.e., 400 mm) was used to carry out the two-dimensional simulation (plane strain) of the strip footing on the wall.

**2. 7. Sample Preparation** The overall height of the wall in the model test was 450 mm that represents a wall with 1.8 m height in real scale. This height is acceptable for GRS bridge abutment as used by Adams and Saunder [34]. The reinforcement layers spacing and the soil friction angle has the greatest effect on the geosynthetic tensile forces [35]. In order to obtain higher ultimate passive force in GRS abutment, Ramalakshmi and Dodagoudar [36] found that the reinforcement layers spacing should be closer. However, in most cases, the spacing is chosen by the requirement of the project.

In this study, four geosynthetic layers were used at a spacing of 90 mm. To avoid pull-out effects, length of 510 mm was adopted for the reinforcement layers. The backfill was compacted in 2-cm layers with an optimum moisture content of 2.5% and a relative density about 70%. In all the tests containing the sand-tire shred mixture, the tire shred was used at a mass replacement rate of 7.5% with a rate in the range of 6% to 10%, as recommended by previous work [37, 38]. Moreover, a greased transparent polyethylene plastic sheet was placed on both of the inner sides of the box to eliminate the effects of the sidewalls on the sample.

## 3. EXPRIMENTAL PROGRAM

**3. 1. Loading Pattern** Overall, two series of tests were performed under different loading conditions. In the first series, the samples were subjected to monotonic loading, and the loading continued until failure has reached. Four monotonic tests were performed, i.e., three tests on sand backfill, and one on a mixture of sand and tire shreds. In those three tests, the samples were quite similar, and only the location of the strip footing was different. In the second series of experiments, the samples were first subjected to vertical cyclic loading, and then, after some delay and then unloading, they were subjected to monotonic loading until failure. The amplitude of the cyclic loading was selected as a percentage of the monotonic bearing capacity; a method that was used by previous studies [39-41]. Cyclic tests were initially loaded monotonically at 20% of $q_u$ ($q_u$ is the ultimate bearing capacity of the monotonic sand test when D=1B), and then, they were loaded with three different stress levels (i.e., 0.2 $q_u$, 0.4 $q_u$, and 0.6 $q_u$). Accordingly, 200 cycles were applied to each sample at the frequency of 0.1 Hz at every stress level (i.e., a total of 600 cycles for each sample). Islam and Gnanendran [42] reported that for a particular loading amplitude, the footing settlement slightly changed (by about 10 to 15%) with an increase in loading frequency from 0.2 to 5 Hz, and the effects became more evident at a higher loading frequency. Therefore, having a loading frequency of 0.1 Hz for the model has a negligible effect on the results. Three cyclic loading tests were conducted on GRS without tire shred, while one was performed on a backfill made of the sand-tire shred mixture. Figure 3 displays the loading pattern. Table 4 presents the testing program examined in this work.

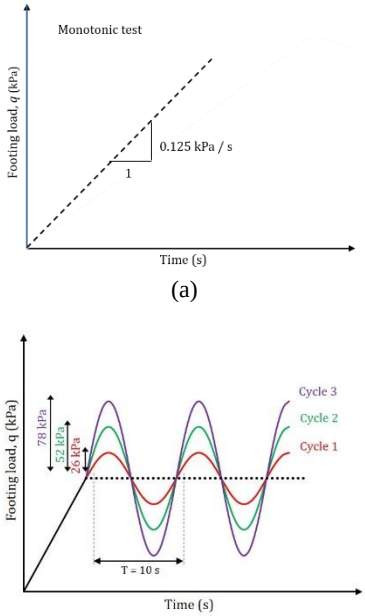


**Figure 3.** Loading pattern, a) monotonic loading, b) vertical cyclic loading

**TABLE 4.** Model test program

| Type | Backfill material | Footing distance from facing | $q_s/q_u$ (%) | $q_c/q_u$ (%) |
|---|---|---|---|---|
| Monotonic | sand | 1B, 2B, 3B | - | - |
| Monotonic | sand-tire shred | 2B | - | - |
| yclic | Sand | 1B, 2B, 3B | 20 | 20, 40, 60 |
| Cyclic | sand-tire shred | 1B, 2B, 3B | 20 | 20, 40, 60 |
| Monotonic (post-cyclic) | sand | 1B, 2B, 3B | - | - |
| Monotonic (post-cyclic) | sand-tire shred | 2B | - | - |

$q_u$=The ultimate bearing capacity of the monotonic sand test when D=1B
$q_s$=The initial monotonic loading
$q_c$=The cyclic loading amplitude

**3. 2. Repeatability Test** To check the repeatability of the results, the footing was placed at a distance of 2B from the facing, and then, two tests were carried out. The results for the bearing capacity against the footing settlement both showed the same behavior when repeated (Figure 4).

## 4. TEST RESULTS AND DISCUSSION

The results of the tests are presented in three categories, regardless of the backfill material, i.e., monotonic loading, cyclic loading, and post-cyclic loading behavior. In each section, the behaviors of the models with the sand backfill are discussed. Then, the results for the sand-tire shred mixture are given and discussed.

**4. 1. Monotonic Loading** Figure 5 displays the results of model test with pure sand backfill under failure conditions. Based on the results, the dominant failure mode for short distances between the footing and the wall facing (D=B) was related mainly to the failure of the wall facing (see Figure 12(a)). Moreover, with an increase in the distance from the facing, the role of the geosynthetic layers in the footing bearing capacity becomes more significant. At a long distance (D=3B) from the facing, the wall continued to carry until the geosynthetic ruptured, and then the sample has been failed. At D=2B and 3B, the failure first initiated at the corners of the strip footing, and it progressively mobilized toward the center of the wall. Khosrojerdi et al. [43] also have reported this observation for the sliding between the soil and the geotextile layers in GRS walls.

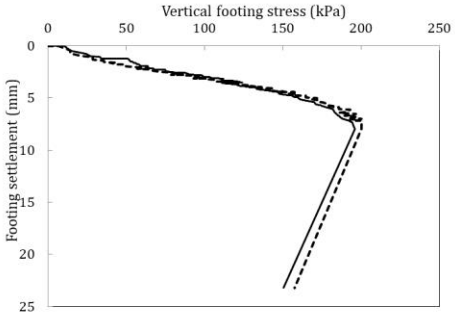


**Figure 4.** Result for two samples with the same properties

The variations in the footing settlement versus the vertical stress on the footing at different footing placement distances are displayed in Figure 5(a). As shown in this figure, with an increase in the distance between the footing and the facing, the maximum bearing capacity of the footing increases. Under different footing placement conditions, i.e., distances of B, 2B, and 3B, the maximum ultimate bearing capacity of the footing (regardless of the footing settlement) is 130, 210, and 230 kPa, respectively. Xiao et al. [32] stated that at distances of more than 0.4 of the wall height (D/H > 0.4), the bearing capacity of the footing remained constant. In the present study, the value of D/H for various locations of the footing (i.e., distances of 1B, 2B, and 3B) is 0.16, 0.34, and 0.5, respectively. The results indicate that by increasing the D/H to 0.5, the bearing capacity continues to be increased. However, an increase in bearing capacity from 2B to 3B is very small. It is worth noting that the load increases with a slope pertinent to the deformations. The slope of the load-deformation curve decreases with an increase in the distance between the footing and the wall facing. This means that the behavior of the reinforced soil approaches the ductile behavior with an increase in the distance from the wall facing, which can be attributed to the type of failure governing the model. When the footing is located at a distance of B from the facing, the local failure in the wall leads to a decrease in bearing capacity and extensive deformations in the footing. At this distance, heavy sliding occurs between the soil and the geosynthetic layer, and the load cannot be transferred to the lower layers of the wall. At this distance, the softening regime governing the GRS is mainly caused by the decrease in the sand shear strength, which leads to in the sliding of the upper layers of the facing blocks, and ultimately causes them to fall (see Figures 6(a) and 12(a)). Xie et al. [44] called this mechanism a log-spiral wedge and occurred when the footing is located closer to the facing or the GRS wall is tall. However, when the footing is at the distance of 3B from the facing, the footing bearing capacity is independent of the wall facing deformations, and the footing experiences collapsibility due to the geosynthetic rapture (see Figures 6(c) and 12(c)) and two-sided general shear mechanism is governing [44]. As a result, the flexible behavior of the geosynthetic

dominates the reinforced soil system. The failure in the soil beneath the footing is affected by the geosynthetic flexibility behavior with an increase in the load. However, regardless of the position of the footing, the GRS (without any connection between the reinforcement layers and the blocks) experiences the internal sliding type of failure at the end of the loading process (see Figure 12). This failure mode was discussed in literature [44, 45].

Since the lateral deformation is an important parameter in the stability assessment and construction of GRS walls, the changes in the horizontal displacement in the facing in relation to the footing settlement were recorded for two locations in the wall, i.e., the middle and the upper quarter parts of the wall, as depicted in Figures 1(b), 5(b) and 5(c). The horizontal displacement in the upper quarter of the wall in all the models is almost two times that of the middle of the wall. As noted by Mirmoradi and Ehrlich [10] the locations of the surcharge and footing change the deformation profile of the wall facing. The results show that the location of the surcharge has a significant impact on the lateral displacement of the facing. The lateral displacement in the samples placed at the distances of B and 2B has been increased linearly with an increase in the footing settlement to 0.7% and 1.8% of the wall height, respectively. Thereafter, the lateral deformation in the wall facing remained unchanged up to a settlement of approximately 4-5% of the wall height. This outcome can be attributed to the interlocking of the soil and the geosynthetic layers. In the initial deformations in the reinforced soil, the reinforcement layers did not start functioning yet, and the initial settlement was caused by the soil deformations. Immediately, the interaction between the soil and the geosynthetic has been commenced. With an increase in the footing settlement from 0.7% (for the distance of 1B) and 1.8% (for distances of 2B and 3B) to approximately 4-5%, a large fraction of the footing stresses and deformations have been transferred to the reinforced soil, and the wall facing did not deform. Then, as the settlement exceeded the wall bearing capacity threshold, the lateral deformations become larger, indicating the onset of the failure of the reinforced soil. This trend was observed in the upper quarter of the wall due to the size of the shallow foundation, and considerable deformations did not occur in the middle of the walls as stated by Ahmadi and, Hajialilue-Bonab [46] and Li et al. [47]. Interestingly, an increase in the deformations in the middle of the wall has occurred in the farthest footing (3B distance), as compared to the adjacent footings. Since the failure mode in this footing resulted in from a decrease in the strength of the soil beneath the footing (the effect of the facing failure on the bearing capacity is smaller), a large part of the stress was transferred to the depth of the soil until the geosynthetic has been raptured (see Figure 6(c)) and the deformations in the middle of the wall facing grew.

Another test was performed to improve the behavior of the reinforced soil at the distance of 2B from the facing inner edge by adding tire shred to the backfill. In

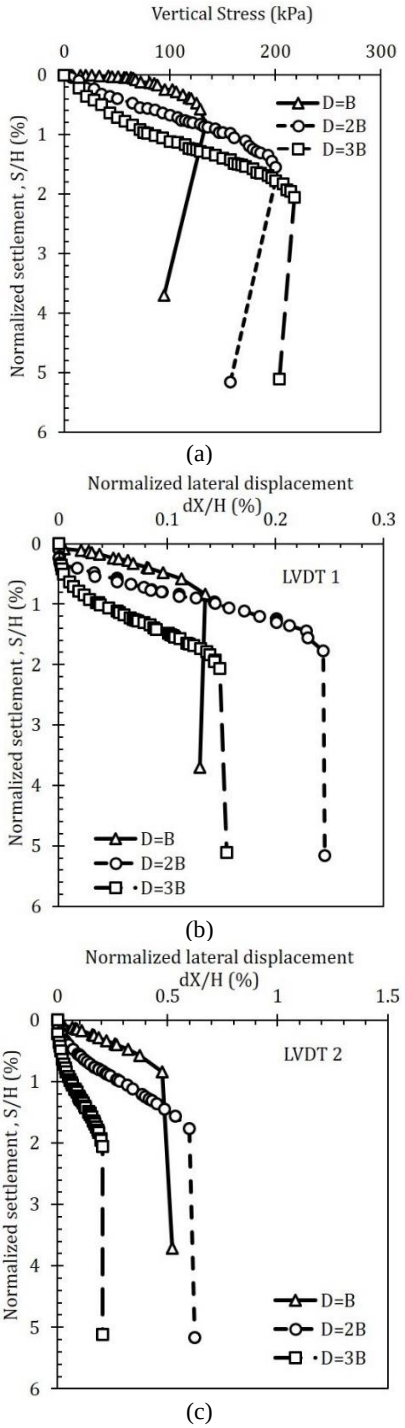


**Figure 5.** Results of monotonic loading tests on sand backfill, a) vertical stress vs. normalized vertical settlement, b, c) normalized lateral displacement vs. normalized vertical settlement at 0.5H and 0.75H, respectively

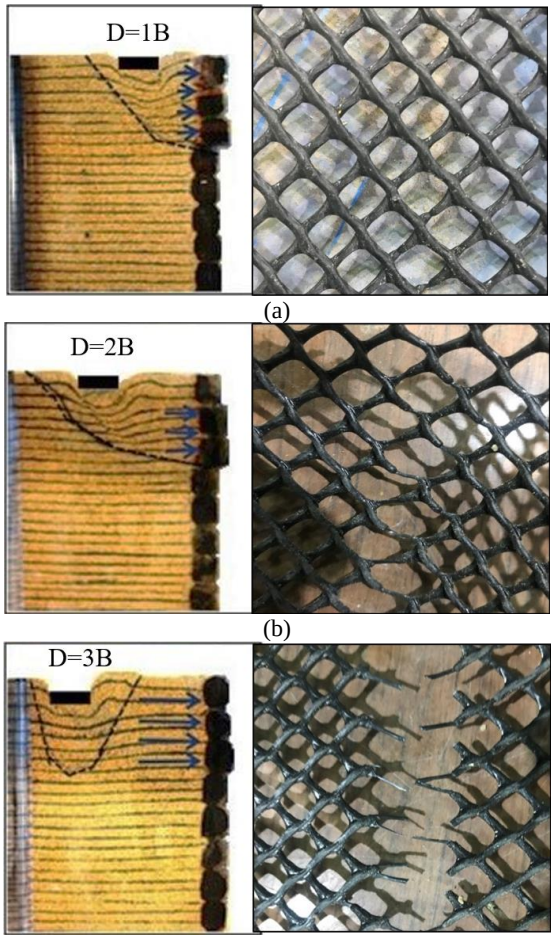


**Figure 6.** Deformation at the top layer of the geosynthetic after monotonic loading at a) D=1B, b) D=2B, and c) D=3B

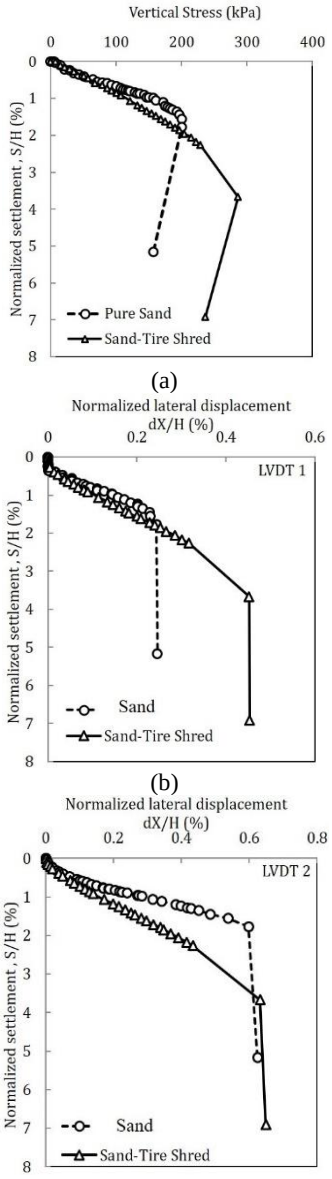


**Figure 7.** Results of monotonic loading tests on sand and sand-tire shred mixture, a) vertical stress vs. normalized vertical settlement, b, c) normalized lateral displacement vs. normalized vertical settlement at 0.5H and 0.75H, respectively

Figures 12(b) and 12(d), the failure mode of the wall is displayed for two states, i.e., first without tire shred, and second with sand-tire shred mixture. When the sand-tire shred mixture is used, the pressure is reduced, as noted by previous works [23,48]. The sample is exposed to more pressure, and the bearing capacity increases to approximately 290 kPa, which is almost 38% higher than the behavior of the pure sand sample (Figure 7(a)). Figures 7(b) and 7(c) demonstrate that the lateral deformations in both samples are similar before reaching a settlement of 1.7%. Afterward, the tire shred contributes to the bearing process, increasing the ductility of the lower middle part of the wall. In the upper-middle part of the wall, the deformation behavior of the sample has a milder slope, indicating that the tire shred grains take part in the bearing mechanism, and a larger load is transferred to the lower layers of the reinforced soil, which is visible in the form of distortions in the lower layer. Using 3D numerical modeling; Mahgoub and El Naggar [49] reported that tire shreds resulted in an improvement in transferring the stresses, reducing the stress influence zone underneath the footing.

**4. 2. Cyclic Loading** After the monotonic loading tests series, the new samples were tested under cyclic loading at three different stress levels. First, 20% of $q_u$ ($q_u$ is the ultimate bearing capacity of the monotonic test when D=1B) was considered as the dead load. Then, at each footing position, three different stress levels, i.e., 0.2, 0.4, and 0.6 of $q_u$, were applied to simulate the cyclic loadings. To this end, 200 cycles were applied to

the samples at each stress level. Figure 8 presents the values of the lateral displacement and the settlement of the footing in the GRS wall samples for three locations of the footing. In the GRS with pure sand backfill (Figures 8(a), 8(b) and 8(c)), it is observed that from cycles up to 15, the rate of the lateral deformation is almost sharp. However, as the number of cycles increases, this rate decreases. While from cycle 100 to the end, it grows slowly or remains constant. Alam et al. [50] state that the majority of the footing displacements and soil stresses occur within the primary loading cycles. In sand-tire shred mixture samples (Figures 8(d), 8e, and 8f) at a high-stress level (0.6 qu), the lateral deformations of the samples continue to increase, and reach a constant value after more cycles. It is also observed that at the same stress level, the lateral deformation decreases in all GRS walls by increasing the footing distance from the facing. In the GRS with pure sand backfill at small (0.2 $q_u$) and medium (0.4 $q_u$) stress levels, the value of the lateral deformation has increased to 1.5 to 3 times that of the case where the sand-tire shred mixture is used. In the sand-tire shred mixture samples at a high-stress level (0.6 $q_u$) for the location of footing at D=1B, the value of lateral displacements increases to 1.5 to 2 times that of the pure sand samples. The residual settlement at small and medium stress levels for the pure sand samples is

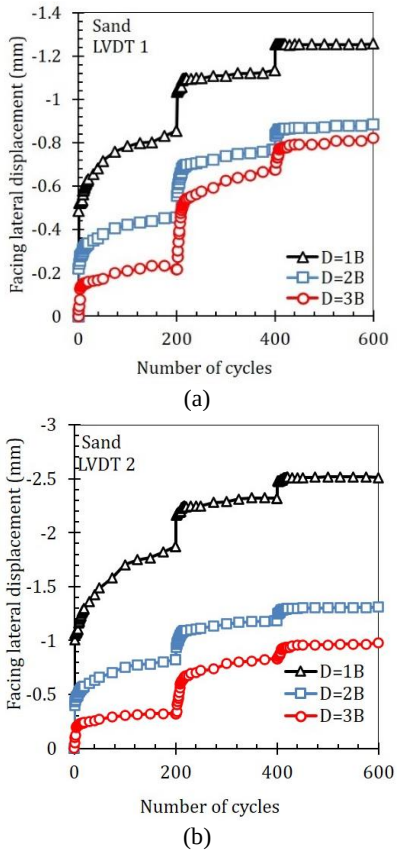


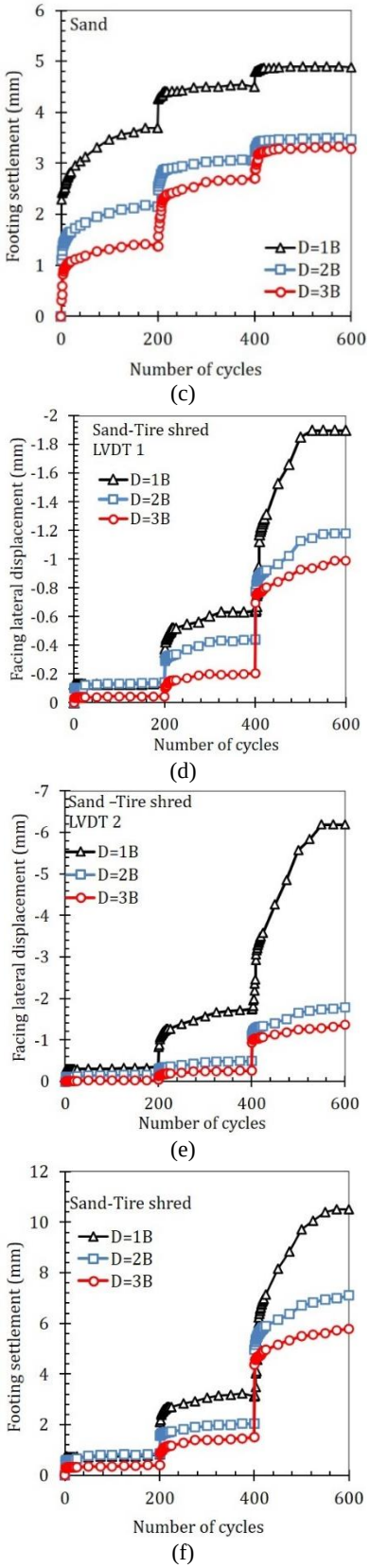


**Figure 8.** Results of cyclic loading: (a, b and c) on backfill without tire shred, (d, e and f) on sand-tire shred mixture backfill

higher; however, at a large stress level, this value for the sand-tire shred mixture is almost two times that of the pure sand samples.

Figure 9 shows the lateral deformation profile of the facing for all locations of footing at different stress levels. Regardless of the backfill material, with an increase in distance from the facing, the lateral deformation of the facing decreases. Also, with an increase in stress level in the cyclic loading without considering the location of the footing, the lateral deformation of the wall facing increases. Interestingly, the lateral deformation of sand-tire shred mixture GRS at low and medium stress levels is less than sand GRS wall, but at high-stress levels, it causes inverse behavior irrespective of the location of the footing.

**4. 3. Post-Ccyclic Loading** Following the cyclic loading, the monotonic loading of the samples was carried out at each position in the strip footing. Figure 12 presents the wall failure modes. According to these results, the wall deformations have increased at the end of the test. The bearing capacity of the specimens located at the distances of 2B and 3B has increased by approximately 23 and 26%, as compared to the pre-cyclic loading state, respectively (Figure 10(a)). However, in the sample at the least distance (B), the bearing capacity remained almost unchanged because of the very large effect of the wall facing on the sample under cyclic loading. As shown in Figures 10(b) and 10(c), the lateral deformations in the upper-middle part have increased, while they have decreased in the lower-middle part, except for the samples located at very short distances. In the upper half of the wall, lateral deformations have occurred in samples placed at the distances of B and 2B with an increase in stress. Consequently, the sliding mode and the internal instability of the wall are observed.

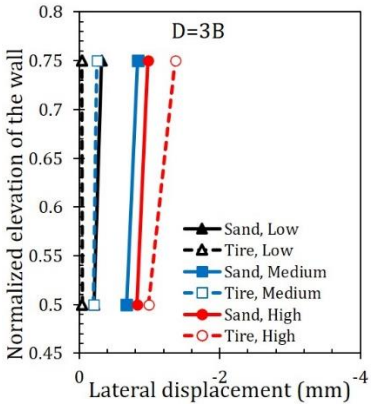


(c)

**Figure 9.** Lateral displacement profile of the facing in three stress levels (low, medium and high) different location of the footing a) D=1B, b) D=2B and c) D=3B

There are continued settlements in the footing with an increase in stress in the GRS containing tire shred (Figure 11). The sample experiences settlement from the onset of the loading due to the ductility of the tire shreds. However, this settlement is accompanied by little lateral deformation in the upper part of the wall up to a settlement of approximately 1.3%. Therefore, the footing settlements are reversible, and the lateral deformations in the wall are postponed until the sample

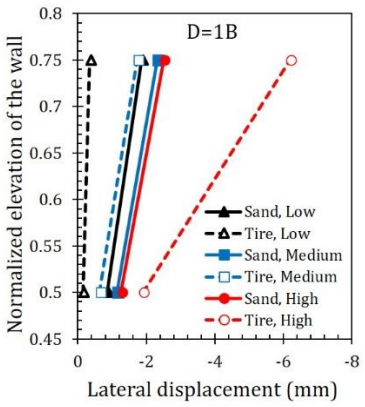


(a)

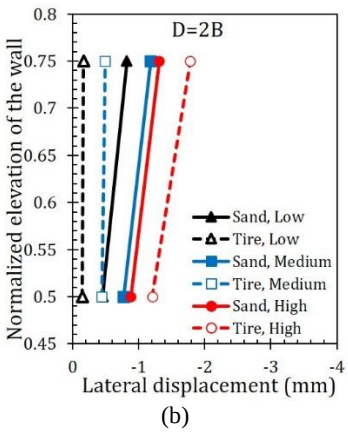


(b)

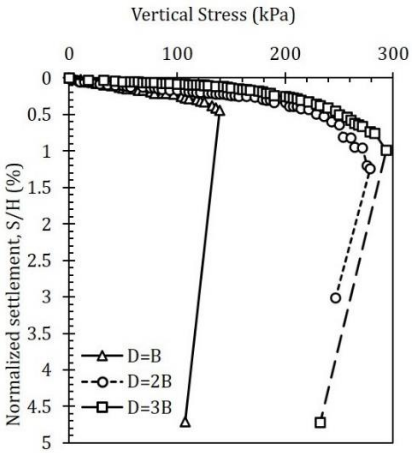


(a)

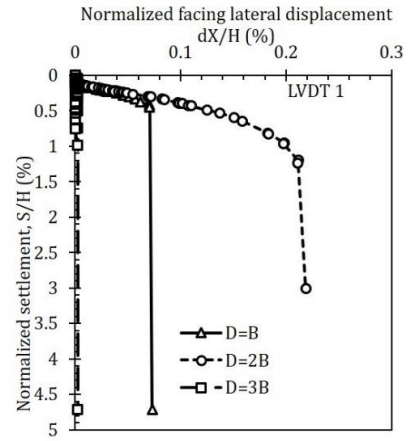


(b)

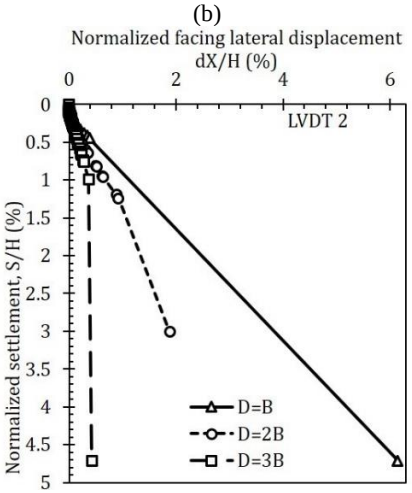


(c)

**Figure 10**. Results of post- cyclic loading on sand backfill, a) vertical stress vs. normalized vertical settlement, b, c) normalized lateral displacement vs. normalized vertical settlement at 0.5H and 0.75H, respectively

exceeds 90% of the peak strength. However, dX/H in the sand samples at the peak strength is approximately 1%, and it continues with the same rate until failure.

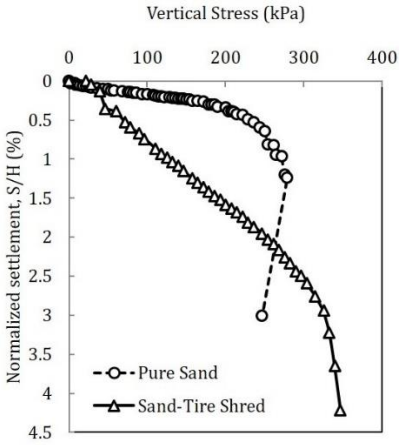


(a)

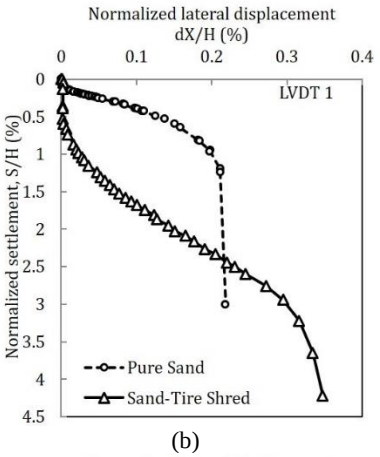


(b)

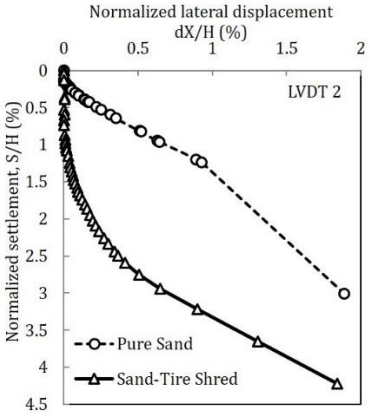


(c)

**Figure 11**. Results of post-cyclic loading tests on sand and sand-tire shred mixture, a) vertical pressure vs. normalized vertical settlement, b, c) normalized lateral displacement vs. normalized vertical settlement at 0.5H and 0.75H, respectively

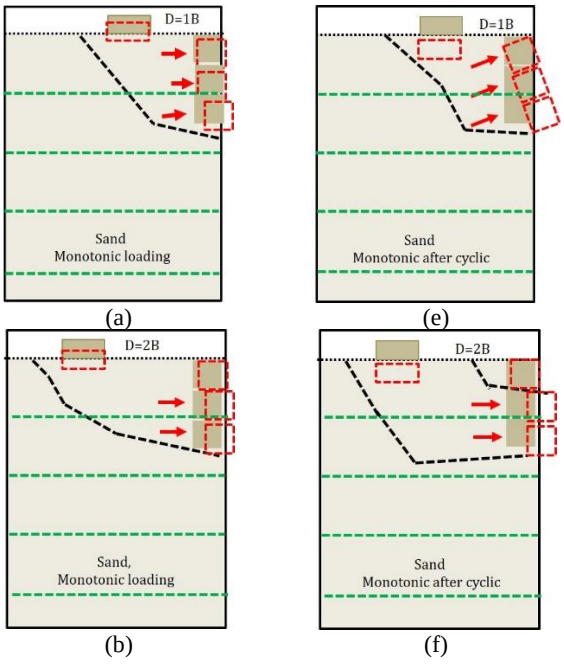


(a) (e) (b) (f)

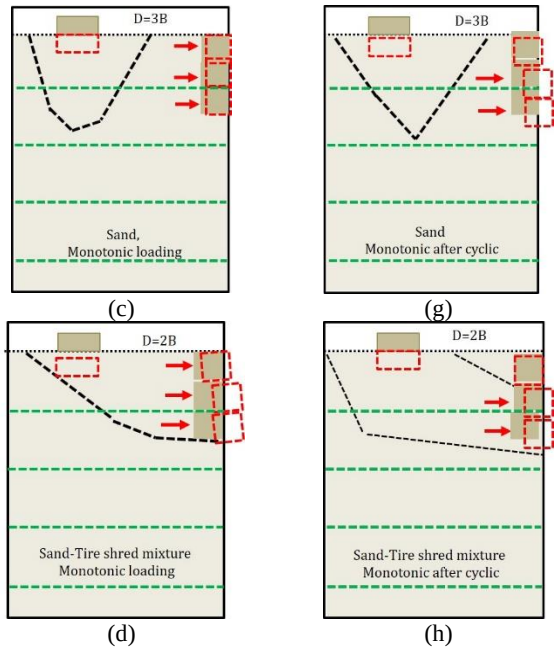


**Figure 12**. Failure modes for the strip footing on the GRS wall under monotonic loading before (a, b, c, d) and after cyclic loading (e, f, g, h), (drawn based on Figure 6)

The behavior of walls in monotonic and monotonic post-cyclic loading at different levels of vertical strain is illustrated in Figure 13. Figure 13(a) shows the vertical stress-vertical strain curve for the footing located on the wall. As it is observed, at the same strain levels, sand GRS presents more strength, but sand-tire shred GRS have displayed more strain due to their high ductility and increasing more resistance. Also, the monotonic post-cyclic behavior of the sand GRS, despite its higher strength, had less ductility, but in the GRS including the tire shred, the value of the change in strength and decrease in ductility is negligible.

The behavior of the lateral wall strain profiles for different percentages of vertical strain for monotonic and monotonic post-cyclic loading are demonstrated in Figures 13(b) and 13(c), respectively. At the same vertical strain levels, the sample with the tire shred indicates less horizontal strain. The sand GRS has been failed at lower strain levels. Table 5 presents a summary to compare sand and sand-tire shred mixture parameters.

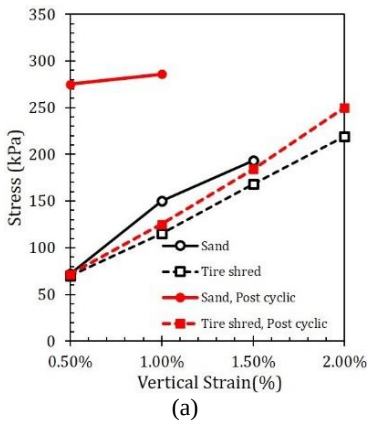


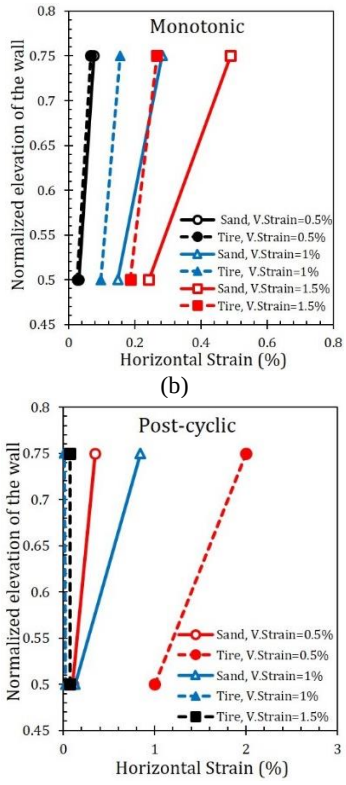


**Figure 13.** The behavior of walls in monotonic and monotonic post-cyclic loading at different levels of vertical strain a) the vertical stress-vertical strain curve, b and c) the behavior of the lateral wall strain profiles for different percentages of vertical strain in monotonic and post cyclic loading

## 5. CONCLUSIONS

Experimental physical models were constructed to investigate the performance of the GRS walls subjected to monotonic and cyclic loadings. The wall facing was made of concrete blocks, and four layers of geosynthetic

**TABLE 5.** comparison of sand and sand-tire shred mixture

| Test result | Pure sand | Sand-tire shred mixture |
|---|---|---|
| Ultimate bearing capacity, kPa | 210 | 290 |
| Maximum lateral deformation, mm | 2.7 | 2.9 |
| Bearing capacity at 0.5% vertical strain, kPa | 68 | 68 |
| Bearing capacity at 1% vertical strain, kPa | 155 | 117 |
| Bearing capacity at 1.5% vertical strain, kPa | 192 | 171 |

were used in the reinforced soil wall. The effects of the position of the strip footing, stress level and sand-tire shred admixture on the lateral deformations of the wall facing, bearing capacity and the settlement beneath the footing were studied. The following conclusions can be made based on the findings from this study; however, they are limited to cases similar to those physical models considered in this study:

- The stress level significantly influenced the lateral wall deformations at the near facing footing. However, the effects of the stress level on the lateral deformations decrease drastically at far footings. The local failure of the wall was the dominant failure mode in the near facing footing. However, with an increase in the distance from the wall facing, the failure mode is shifted to internal sliding.
- Using the sand-tire shred admixture, the bearing capacity of the footing on the GRS wall was increased. Moreover, at small stress levels, the deformation behaviour of the tire shred GRS wall is more appropriate than the sand GRS wall; but at high stress levels, the deformation behaviour of the shred tire GRS is higher than that of the sand GRS.
- At post cyclic loading the bearing capacity of the samples placed at the longer distances from the facing has increased in comparison to the monotonic loading samples. However, at the short distance, the bearing capacity remains almost unchanged.

It is worthy to note that, the frequency effect and the connection between the facing blocks and geosynthetic layers are not considered. Besides, the findings are based on 12 small-scale model tests. The applicability of the results to other situations required further investigation.

## 6. ACKNOWLEDGMENTS

Funding received from Shahid Beheshti University (SBU) grant and the Sad Afzar company, is gratefully acknowledged.

## 7. REFERENCES

1. Aggarwal, P., Sharma, K. G., Gupta K. K., "Modeling of unreinforced and reinforced pavement composite material using HISS model", ***International Journal of Engineering***, Vol. 20, No. 1, (2007), 13-22.
2. Abbaszadeh, R., Vafaeian, M., "Laboratory model tests to study the behavior of soil wall reinforced by weak reinforcing layers", ***International Journal of Engineering***, Vol. 21, No. 4, (2008), 361-374.
3. Bahrami, M., Marandi S. M., "Large-scale experimental study on collapsible soil improvement using encased stone columns", ***International Journal of Engineering***, Vol. 34, No. 5, (2021), 1145-1155, DOI: 10.5829/ije.2021.34.05b.08.
4. Ehrlich, M., Mirmoradi SH. "Evaluation of the effects of facing stiffness and toe resistance on the behavior of GRS walls", ***Geotextile and Geomembranes*** Vol. 40, (2013), 28-36, DOI: 10.1016/j.geotexmem.2013.07.012.
5. Mirmoradi, SH., Ehrlich, M. "Evaluation of the effect of toe restraint on GRS walls", ***Transportation Geotechnics***, Vol. 8, (2016), 35-44, DOI: 10.1016/j.trgeo.2016.03.002.
6. Ehrlich, M., Mirmoradi, SH., Saramago, RP. "Evaluation of the effect of compaction on the behavior of geosynthetic-reinforced soil walls", ***Geotextile and Geomembranes,*** Vol. 34, (2012), 108-115, DOI: 10.1016/j.geotexmem.2012.05.005.
7. Zheng, Y., Fox, PJ., McCartney, JS. "Numerical study of the compaction effect on the static behavior of a geosynthetic reinforced soil-integrated bridge system", ***Geotechnical Speccial Publications***, (2017), 33-43, DOI: 10.1061/9780784480458.004.
8. Mirmoradi, SH., Ehrlich, M., Chinchay, P., Dieguez, C. "Evaluation of the combined effect of facing inclination and uniform surcharge on GRS walls", ***Geotextile and Geomembranes***, Vol. 47, No. 5, (2019), 685-691, DOI: 10.1016/j.geotexmem.2019.103485.
9. Doger, R., Hatami, K. "Influence of facing on the performance of GRS bridge abutments", ***International Journal of Geosynthetics and Ground Engineering***, Vol. 6, No. 4, (2020), DOI: 10.1007/s40891-020-00225-y.
10. Helwany, SMB., Wu, JTH., Kitsabunnarat, A. "Simulating the behavior of GRS bridge abutments", ***journal of Geotechnical and Environmental Engineering***, Vol. 33, (2007), 1229-1240, DOI: 10.1061/(ASCE)1090-0241(2007)133:10(1229).
11. Zheng, Y., Fox, PJ. "Numerical investigation of geosynthetic-reinforced soil bridge abutments under static loading", ***Journal of Geotechnical and Environmental Engineering***, Vol. 142, (2016), 1-13, DOI: 10.1061/(ASCE)GT.1943-5606.0001452.
12. Ardah, A., Abu-farsakh, M., Voyiadjis, G. "Numerical evaluation of the performance of a geosynthetic reinforced soil-integrated bridge system (GRS-IBS) under different loading conditions", ***Geotextile and Geomembranes***, Vol. 45, No. 6, (2017), 558-569, DOI: 10.1016/j.geotexmem.2017.07.005
13. Abu-Farsakh, M., Ardah, A., Voyiadjis, G. "Numerical investigation of the performance of a geosynthetic reinforced soil-integrated bridge system (GRS-IBS) under working stress conditions", ***Geotechnical Special Publications***, (2018), 76-87, DOI: 10.1061/9780784481608.008.
14. Mirmoradi, SH., Ehrlich, M. "Experimental evaluation of the effects of surcharge width and location on geosynthetic-reinforced soil walls", ***International Journal of Physical Modelling in Geotechnics***, Vol. 19, (2019), 27-36, DOI: 10.1680/jphmg.16.00074.
15. Helwany, SMB., Reardon, G., Wu, JTH. "Effects of backfill on the performance of GRS retaining walls", ***Geotextile and Geomembranes***, Vol. 17, (1999), 1-16, DOI: 10.1016/S0266-1144(98)00021-1.
16. Hatami, K. "Parametric analysis of reinforced soil walls with different backfill material properties", Geo engineering centre at queen's-RMC royal military college of Canada, (2005).
17. Hatami, K., Witthoeft, AF. "A numerical study on the use of geofoam to increase the external stability of reinforced soil walls", ***Geosynthetic International***, Vol. 15, (2008), 452-470, DOI: 10.1680/gein.2008.15.6.452.
18. Zheng, Y., Fox, PJ., McCartney, JS. "Numerical simulation of deformation and failure behaviour of geosynthetic reinforced soil bridge abutments", ***Journal of Geotechnical and Environmental Engineering***, Vol. 144, No. 7, (2018), DOI: 10.1061/(ASCE)GT.1943-5606.0001893.
19. Wu, JTH., Ooi, PSK. "Synthesis of geosynthetic reinforced soil (GRS) design topics", HWA-HRT-14-094, Federal Highway Administration, Washington, D.C., USA., (2015),

20. Xiao, C., Han, J., Zhang, Z. "Experimental study on performance of geosynthetic-reinforced soil model walls on rigid foundations subjected to static footing loading", ***Geotextile and Geomembranes***, Vol. 44, (2016), 81-94, DOI: 10.1016/j.geotexmem.2015.06.001.
21. Masad, E., Taha, R., Ho, C., Papagiannakis, T. "Engineering properties of tire/soil mixtures as a lightweight fill material", ***Geotechnical Testing Journal***, Vol. 19, (1996), 297-304, DOI: 10.1520/GTJ10355J.
22. Chaney, R., Demars, K., Feng, Z-Y. Sutter K. "Dynamic properties of granulated rubber/sand mixtures", ***Geotechnical Testing Journal***, Vol. 23 No. 3, (2000), 338-344, DOI: 10.1520/GTJ11055J.
23. Xiao, M., Bowen, J., Graham, M., Larralde, J. "Comparison of seismic responses of geosynthetically reinforced walls with tire-derived aggregates and granular backfills", ***Journal of Materials in Civil Engineering***, Vol. 24, (2012), 1368-1377, DOI: 10.1061/(ASCE)MT.1943-5533.0000514.
24. Iai, S. "Similitude for shaking table tests on soil-structure-fluid model in 1g gravitational field", ***Soils and Foundations***, Vol. 29, (1989), 105-118, DOI: 10.3208/sandf1972.29.105.
25. Komak Panah, A., Yazdi, M., Ghalandarzadeh, A. "Shaking table tests on soil retaining walls reinforced by polymeric strips", ***Geotextile and Geomembranes***, Vol. 43, (2015), 148-161, DOI: 10.1016/j.geotexmem.2015.01.001.
26. Latha, GM., Santhanakumar, P. "Seismic response of reduced-scale modular block and rigid faced reinforced walls through shaking table tests", ***Geotextile and Geomembranes***, Vol. 43, (2015), 307-316, DOI: 10.1016/j.geotexmem.2015.04.008.
27. ASTM D422-63. "Standard test method for particle-size analysis of soils", ASTM International, West Conshohocken, PA, USA., (2007).
28. Maroof, MA., Mahboubi, A., Noorzad, A., Safi, Y. "A new approach to particle shape classification of granular materials", ***Transportation Geotechnics***, Vol. 22, (2020), DOI: 10.1016/j.trgeo.2019.100296.
29. ASTM D4253. Standard test methods for maximum index density and unit weight of soils using a. ASTM International, West Conshohocken, PA, USA., (2006).
30. Indraratna, B., Sun, Q., Grant, J. "Behaviour of subballast reinforced with used tyre and potential application in rail tracks", ***Transportation Geotechnics***, Vol. 12, (2017), 26-36, DOI: 10.1016/j.trgeo.2017.08.006.
31. ASTM D6637. "Standard Test method for determining tensile properties of geogrids by the single or multi rib tensile method", ASTM International, West Conshohocken, PA, USA. (2010).
32. Xiao, C., Han, J., Zhang, Z. "Experimental study on performance of geosynthetic-reinforced soil model walls on rigid foundations subjected to static footing loading", ***Geotextile and Geomembranes***, Vol. 44 No. 1, (2015), 81-94, DOI: 10.1016/j.geotexmem.2015.06.001.
33. Adams, M., Nicks, J., Stabile, T., Wu, J., Schlatter, W., Hartmann, J. "Geosynthetic reinforced soil integrated bridge system, Synthesis report", 64., (2011).
34. Adams M.T., Saunders S.A. "Upper ouachita national wildlife refuge GRS abutments for replacement bridges", Presentation by Adams, M., and Saunders, S.A., FHWA., (2007).
35. Zheng, Y., Fox, PJ., Mccartney, JS. "Numerical study on maximum reinforcement tensile forces in geosynthetic reinforced soil bridge abutments", ***Geotextile and Geomembranes***, Vol. 46, (2018), 634-645, DOI: 10.1016/j.geotexmem.2018.04.007.
36. Ramalakshmi, M., Dodagoudar, GR. "Passive force–displacement behaviour of GRS bridge abutments", ***International Journal of Geosynthetics and Ground Engineering***, Vol. 4, (2018), DOI: 10.1007/s40891-018-0145-7.
37. Prasad, DSV., Raju, GVRP. "Performance of waste tyre rubber on model flexible pavement", ***Journal of Engineering and Applied Science***, Vol. 4, (2009), 89-92.
38. Munnoli, PM., Sheikh, S., Mir, T., Kesavan V, Jha R. "Utilization of rubber tyre waste in subgrade soil", ***IEEE Glob. Humanit. Technol. Conf***. South Asia Satell., IEEE, (2013), 330-333, DOI: 10.1109/GHTC-SAS.2013.6629940.
39. Yeo, B., Yen, SC., Puri, VK., Das, BM., Wright, MA. "A laboratory investigation into the settlement of a foundation on geogrid-reinforced sand due to cyclic load", ***Geotechnical and Geological Engineering***, Vol. 11, (1993), 1-14, DOI: 10.1007/BF00452917.
40. El-Sawwaf, M., Nazir, AK. "Behaviour of repeatedly loaded rectangular footings resting on reinforced sand", ***Alexandria Engineering J*ournal**, Vol. 49, (2010), 349-356, DOI: 10.1016/j.aej.2010.07.002.
41. Moghaddas Tafreshi, SN., Dawson, AR. "Behaviour of footings on reinforced sand subjected to repeated loading- Comparing use of 3D and planar geotextile", ***Geotextile and Geomembranes***, Vol. 28, (2010), 434-447, DOI: 10.1016/j.geotexmem.2009.12.007.
42. Islam, MA., Gnanendran, CT. "Slope stability under cyclic foundation loading - Effect of loading frequency", ***Geo-Congress Reston***, VA: American Society of Civil Engineers, (2013), 750-761, DOI: 10.1061/9780784412787.075.
43. Khosrojerdi, M., Qiu, T., Xiao, M., Nicks, J. "Effects of backfill constitutive behaviour and soil–geotextile interface properties on deformations of geosynthetic-reinforced soil piers under static axial loading", ***Journal of Geotechnical and Environmental Engineering***, Vol. 146, (2020), DOI: 10.1061/(ASCE)GT.1943-5606.0002313.
44. Xie, Y., Leshchinsky, B., Han, J. "Evaluation of bearing capacity on geosynthetic-reinforced soil structures considering multiple failure mechanisms", ***Journal of Geotechnical and Environmental Engineering***, Vol. 145, (2019), DOI: 10.1061/(ASCE)GT.1943-5606.0002072.
45. Bathurst, RJ. "Challenges and recent progress in the analysis, design and modelling of geosynthetic reinforced soil walls", ***10th International Conference of Geosynthetic*** *ICG* (2014).
46. Ahmadi, H., Hajialilue-Bonab, M., "Experimental and analytical investigations on bearing capacity of strip footing in reinforced sand backfills and flexible retaining wall", ***Acta Geotechinca***, Vol. 7, (2012), 357-373, DOI: 10.1007/s11440-012-0165-8.
47. Li, L-H., Yu, C-D., Xiao, H-L., Feng, W-Q., Ma, Q., Yin, J-H. "Experimental study on the reinforced fly ash and sand retaining wall under static load", ***Construction and Building Materials***, Vol. 248, (2020), DOI: 10.1016/j.conbuildmat.2020.118678.
48. Mahgoub, A., El Naggar, H. "Innovative application of tire-derived aggregate around corrugated steel plate culverts", ***Journal of Pipeline Systems and Engineering Practices***, Vol. 11, (2020), Article 04020025, DOI: 10.1061/(ASCE)PS.1949-1204.0000466.
49. Mahgoub, A., El Naggar, H. "Shallow foundations on lightweight TDA backfill: Field tests and 3D numerical modelling", ***Computers and Geotechnics***, Vol. 126, (2020), DOI: 10.1016/j.compgeo.2020.103761.
50. Alam, MJI., Gnanendran, CT., Lo, SR. "Modelling the settlement behaviour of a strip footing on sloping sandy fill under cyclic loading conditions", ***Computers and Geotechnics***, Vol. 86, (2017), 181-92, DOI: 10.1016/j.compgeo.2017.01.010.

## Persian Abstract

**چکیده**

در این مقاله، رفتار مکانیکی دیواره های خاک مسلح ژئوسنتتیکی (GRS) با استفاده از مدل سازی فیزیکی تحت بارهای مونوتونیک و سیکلی ناشی از پی نواری در مسیرهای مختلف تنش بررسی شده است. تأثیر محل قرارگیری پی، سطح تنش، رفتار مونوتونیک نمونه ها پس از بارگذاری سیکلی و استفاده از مخلوط ماسه–خرده تایر بر روی تغییر شکل های جانبی رویه دیوار، ظرفیت باربری و نشست پی نواری مورد بررسی قرار گرفت. برای این منظور، ۱۲ آزمایش مدل فیزیکی با مقیاس ۱:۴ انجام شد. نتایج نشان داد که با افزایش فاصله پی نواری از رویه دیوار و افزودن خرده تایر به مصالح دیوار، ظرفیت باربری افزایش می یابد، اما افزایش ظرفیت باربری ناشی از افزودن خرده تایر به مصالح خاکریز به مراتب بیشتر است. همچنین محل قرارگیری پایه از رویه دیوار پارامتر مهمی در تغییر شکل رویه دیوار و حالت خرابی پی بود. مد غالب گسیختگی برای زمانی که پی در نزدیکی رویه دیوار قرار داشت، به صورت خراب شدن کلی رویه بود اما در حالت قرارگیری پی نواری با فاصله دور از رویه دیوار، پارگی ژئوسنتتیک عامل خرابی مجموعه دیوار و پی نواری بود. همچنین نتیجه آزمایشات بارگذاری سیکلی نشان داد که جابجایی دائمی رویه و نشست باقیمانده پی نواری با سیکل های بار به طور تجمعی افزایش می یابند و اکثر آنها در پانزده سیکل اول رخ می دهند.